LASER & PHOTONICS REVIEWS
www.lpr-journal.org

Pathway Selectivity in 2D Electronic-Vibrational Spectroscopy with Quantum Light

Deependra Jadoun, Hari K. Yadalam, Upendra Harbola, Vladimir Y. Chernyak, Matthias Kizmann, and Shaul Mukamel**

Pathway selectivity in quantum spectroscopy with entangled photons is a powerful spectroscopic tool. Phase-matched signals involving classical light contain contributions from multiple material pathways, whereas quantum spectroscopy may allow the selection of individual pathways. 2D electronic-vibrational spectroscopy (2DEVS) is a four-wave mixing technique which employs visible and infrared entangled photons. It is showed how the three contributing pathways—ground state bleach, excited state absorption, and excited state emission—can be separated by photon-number-resolved coincidence measurements. Entangled photons thus reveal spectral features not visible in the classical signal, with an enhanced spectral resolution.

1. Introduction

Entangled photons[1] offer new avenues in the study of molecules and chemical processes.[2–4] The enhanced two-photon absorption strength of entangled photon pairs (EPPs)[5,6] compared to classical light provides a pivotal manifestation of quantum spectroscopy. The increased entangled two-photon-absorption[7] cross-section stems from the temporal correlation of the EPPs,[8] and the time and energy entanglement of photons can help achieve joint high temporal and spectral spectroscopic resolutions,[9–13] as has been demonstrated in the spectroscopy at conical intersections.[14–16] However, suitably designed classical pulses have been proposed as substitutes for quantum spectroscopy where one photon from an EPP interacts with the sample while the other serves as a reference.[17]

Interferometric[18] EPPs setups have been used for pathway selectivity[19–24] by singling out specific Liouville pathways contributing to the non-linear optical response[25] of material systems. Coincidence photon-counting detection of EPPs has been used to separate different pathways in four-wave mixing.[26,27] Quasiparticle scattering processes have been theoretically selectively probed in exciton transport by using quantum interferometry.[23] Interferometric photon-number-resolved measurements have been used to achieve pathway selectivity in a $\chi^{(2)}$ signal (difference-frequency generation).[24] Three entangled photons have also been used interferometrically to selectively probe individual pathways.[28,29] Recently, pathway selectivity has been proposed using classical pulses in two-dimensional (2D) photon echo spectroscopy.[30]

In this paper, we show how quantum spectroscopy combined with coincidence photon-number-resolved measurement of EPPs may be used to discriminate different contributions to 2D electronic-vibrational spectroscopy (2DEVS) spectra. 2DEVS, proposed by the Graham Fleming group,[31–33] uses two optical pulses followed by two infrared (IR) pulses to probe correlations between electronic and vibrational degrees of freedom in light-harvesting complexes.[34–36] A complement technique 2D vibrational-electronic spectroscopy was proposed by Munira Khalil,[37] which uses two IR pulses followed by two optical pulses to create vibrational transitions. Simpler single-color techniques such as 2D electronic spectroscopy and 2D IR spectroscopy only probe electronic or vibrational transitions, respectively. 2DEVS can explore both electronic and vibrational dynamics. 2DEVS has been used to study energy transfer processes[38–40] and vibronic couplings in light-harvesting complexes.[41–44]

The 2DEVS signal has three contributions: Ground state bleach (GSB), excited state emission (ESE), and excited state absorption (ESA),[25] depicted by Feynman diagrams in **Figure 1b**). GSB reveals vibrational dynamics in the ground electronic state, whereas the ESE and the ESA monitor the vibrational dynamics in the excited electronic state and energy transfer processes. These can be masked by the GSB contributions if the vibrational frequencies in the two electronic states are similar.

D. Jadoun, H. K. Yadalam, M. Kizmann, S. Mukamel
Department of Chemistry
University of California
Irvine, CA 92614, USA
E-mail: matthias.kizmann@web.de; smukamel@uci.edu

D. Jadoun, H. K. Yadalam, M. Kizmann, S. Mukamel
Department of Physics and Astronomy
University of California
Irvine, CA 92614, USA

U. Harbola
Department of Inorganic and Physical Chemistry
Indian Institute of Science
Bangalore 560012, India

V. Y. Chernyak
Department of Chemistry
Wayne State University
5101 Cass Ave, Detroit, MI 48202, USA

V. Y. Chernyak
Department of Mathematics
Wayne State University
656 W. Kirby, Detroit, MI 48202, USA

The ORCID identification number(s) for the author(s) of this article can be found under https://doi.org/10.1002/lpor.202401576

DOI: 10.1002/lpor.202401576

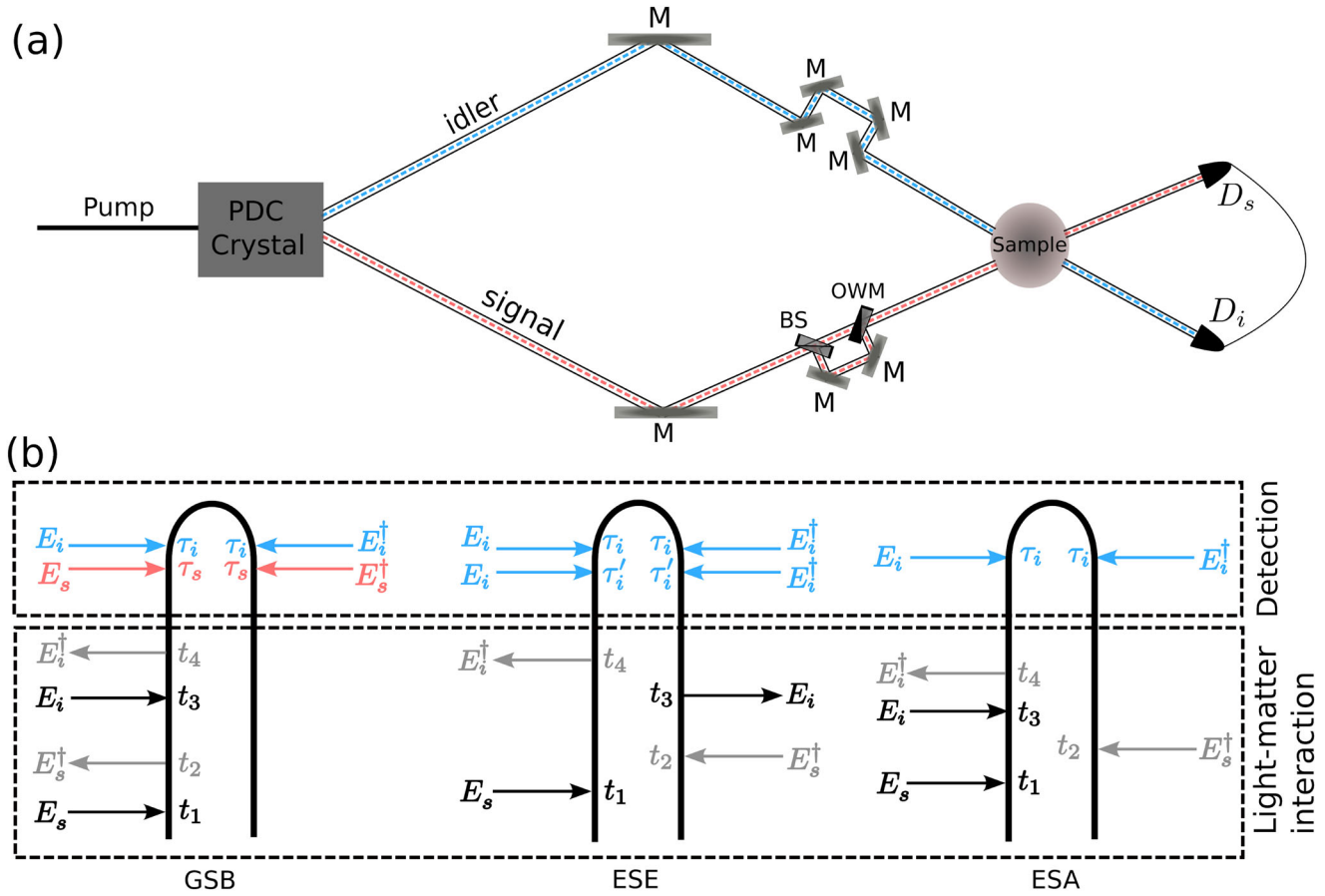

Figure 1. a) The setup that uses EPPs generated by a PDC process in 2DEVS is shown. The *s*-photon and the *i*-photon are directed into two arms of the setup. Sets of mirrors and beam splitters are used in the two arms to vary the path lengths of the *s* and *i* photons, thereby controlling the delays between the photons. The two photons are detected in coincidence after interacting with the sample. Notations: M represents mirror, BS represents beam splitter, and OWM represents one-way mirror. b) Loop diagrams corresponding to GSB, ESE, and ESA processes in 2DEVS are shown. Each loop diagram is divided into two parts: the light-matter interaction part and the detection part. The same colored arrows in the light-matter interaction part belong to the same EPP. In the detection part, blue arrows represent the detection of *i*-photons, and pink arrows represent the detection of *s*-photons.

Here, we show how to separate the three contributions using a photon-number-resolved coincidence measurement with EPPs. The number of signal (*s*) and idler (*i*) photons observed in coincidence can mark a specific 2DEVS pathway. We further explore the effect of the delays of *s*- and *i*-photons for a fixed entanglement time on the spectral resolution along the probe frequency.

2. Theory

2DEVS is a four-wave mixing technique that uses two visible (vis)/ultraviolet (UV) pulses (E_1 and E_2) resonant with vibronic transitions, followed by two IR pulses, E_3 and the signal field (E_s), that induce vibrational transitions within the same electronic state. The signal field, E_s, is emitted in the direction $\mathbf{k}_s = \mathbf{k}_1 - \mathbf{k}_2 + \mathbf{k}_3$, where $\mathbf{k}_1$, $\mathbf{k}_2$, and $\mathbf{k}_3$ are the wavevectors of fields E_1, E_2, and E_3, respectively. We set $\mathbf{k}_1 = \mathbf{k}_2$ so that k_s=k_3, implying self-heterodyne detection.

In our setup depicted in Figure 1a, EPPs generated by the parametric-down conversion (PDC) process are directed into two arms labeled signal and idler, which are in the vis/UV and in the IR regimes, respectively. *s*-photons represent E_1 and E_2 field interactions, and *i*-photons form the E_3 field. A set of mirrors is used in the *i*-arm to control the delay with respect to the *s*-arm photons. An additional pathway is created in the *s*-arm using beam splitters and mirrors, giving rise to a superposition in the *s*-photon state with a variable delay. This allows to mimic the sequence of two vis/UV pulses (E_1 and E_2) in the classical 2DEVS using a single *s*-arm photon. Note that the superposition is between the two pathways that a single *s*-photon can take, and it should not be confused with the superposition of two *s*-photons (see Equation 3). The delay in the *s*-arm (τ_1) is kept smaller than in the *i*-arm (τ_2) so that the *s*- and *i*-photon envelopes are temporally well separated. This can be ensured by setting the delay of *i*-photons larger than the sum of the pump pulse width and the delay in the *s*-arm.

Following the interaction with the sample, the photons in the two arms are detected in coincidence by the detectors D_s and D_i. The photon-number-resolved coincidence measurement is used to select the pathway corresponding to the recorded 2DEVS signal, as depicted in **Table 1**. A one-photon count in each detector D_s and D_i indicates the GSB pathway. Similarly, a zero photon count in D_s and a one photon count in D_i marks the ESA contri-

Table 1. The number of photons detected in each detector is noted for each pathway contributing to 2DEVS.

process \ detector	D_s	D_i
GSB	1	1
ESA	0	1
ESE	0	2

bution. Finally, a zero photon count in D_s and a two-photon count in D_i represents the ESE contribution.

The signal is defined as the coincidence photon-number-resolved measurement of the s-photon and the i-photon,[45,46]

$$S_{QL} = \left\langle \mathbf{T} \frac{\Omega_i^{n_i}}{n_i!} e^{-\Omega_i} \frac{\Omega_s^{n_s}}{n_s!} e^{-\Omega_s} \rho(t) \right\rangle \tag{1}$$

where $\mathbf{T}$ is the time-ordering operator, $\rho(t)$ represents the density matrix for the system at time t, n_i (n_s) is the number of detected i (s) photons, and $\Omega_j = \int \mathrm{d}\tau_j \hat{E}^{\dagger}_{jR}(\tau_j)\hat{E}_{jL}(\tau_j)$ with $\hat{E}_j$ being the electric field superoperator,

$$\hat{E}_j(t) = i\hat{e}\mathcal{E} \int \mathrm{d}\omega_j \hat{a}_j(\omega_j) e^{-i\omega_j t} e^{i\mathbf{k}_j \cdot \mathbf{r}} \tag{2}$$

where $j \in \{s, i\}$, $\hat{e}$ is the polarization, $\mathbf{k}_j$ is the photon wavevector, $\mathcal{E}$ represents the amplitude, $\mathbf{r}$ is the position vector, $\hat{a}_j(\omega_j)$ is the annihilation operator for the j^{th}-photon with frequency ω_j.

The total density matrix ρ is given by the direct product of the molecular, ρ_M, and the field, ρ_F, density matrices. We consider a molecular model system with two electronic states, and a single harmonic vibrational mode that includes five vibrational states in the simulation. The electronic energy gap is 3 eV, and the vibrational frequencies of the ground and excited electronic states are 0.1 and 0.16 eV, respectively. The system Hamiltonian and the energy level diagrams are given in Supporting Information. The molecule is initially in the lowest vibronic state.

The initial field density matrix, $\rho_F = |\psi_F\rangle\langle\psi_F|$, represents the bi-photon entangled state, $|\psi_F\rangle$. We have assumed the following bi-photon wavefunction,

$$|\psi_F\rangle = \int \mathrm{d}\omega_s \int \mathrm{d}\omega_i e^{-(\omega_s+\omega_i-\bar{\omega}_p)^2/2\sigma_p^2} \mathrm{sinc}\left[\frac{(\omega_s-\bar{\omega}_s)}{2}T_s + \frac{(\omega_i-\bar{\omega}_i)}{2}T_i\right] \times (\mathcal{T} + \mathcal{R}e^{i\omega_s\tau_1})\hat{a}_s^{\dagger}(\omega_s)e^{i\omega_i\tau_2}\hat{a}_i^{\dagger}(\omega_i)|0_s, 0_i\rangle \tag{3}$$

where $\bar{\omega}_p$, $\bar{\omega}_s$, and $\bar{\omega}_i$ represent the center frequencies of the pump, the signal, and the idler photons, respectively. σ_p is the pump-pulse bandwidth, T_s (T_i) represents the time spent by the s-photon (i-photon) in the PDC crystal, and $\mathcal{T}$ and $\mathcal{R}$ are transmission and reflection coefficients for the beam splitter in the s-arm, respectively. τ_1 represents the delay between the two paths in the s-arm, and τ_2 is the delay introduced in the i-arm of the setup.

The GSB signal is calculated using Equation (1) with $n_i = 1$, and $n_s = 1$. A perturbative expansion[25] of the total density-matrix in light-matter interaction in Equation (1) leads to the following expression for the signal,

$$\begin{aligned} S_{QL,GSB}(\tau_1,\tau_2) = 2\mathcal{N}\Re\Bigg[&\int_{t_0}^{\infty}\mathrm{d}t_4\int_{t_0}^{t_4}\mathrm{d}t_3\int_{t_0}^{\infty}\mathrm{d}t_2\int_{t_0}^{t_2}\mathrm{d}t_1 \\ &\times\langle\psi_m(t_0)|\,\mu_\nu(t_4)\mu_\nu^{\dagger}(t_3)\mu_e(t_2)\mu_e^{\dagger}(t_1)\,|\psi_m(t_0)\rangle \\ &\times\Phi^*(t_2-\tau_1,t_4-\tau_2)\Phi(t_1,t_3-\tau_2) \\ &+\int_{t_0}^{\infty}\mathrm{d}t_4\int_{t_0}^{t_4}\mathrm{d}t_3\int_{t_0}^{\infty}\mathrm{d}t_2\int_{t_0}^{t_2}\mathrm{d}t_1 \\ &\times\langle\psi_m(t_0)|\,\mu_e(t_1)\mu_e^{\dagger}(t_2)\mu_\nu(t_4)\mu_\nu^{\dagger}(t_3)\,|\psi_m(t_0)\rangle \\ &\Phi^*(t_1,t_4-\tau_2)\Phi(t_2-\tau_1,t_3-\tau_2)\Bigg] \end{aligned} \tag{4}$$

where $\mathcal{N}$ is a normalization factor, $|\psi_m\rangle$ represents the molecular wave-function, μ_ν represents the transition dipole moment (TDM) between vibrational states, μ_e denotes the TDM between electronic states, and $\Phi(t,t')$ is the two-photon amplitude (TPA),

$$\begin{aligned} \Phi(t,t') &= \langle 0_s, 0_i|\,\hat{E}_i(t)\hat{E}_s(t')\,|\psi_F\rangle \\ &= \int \mathrm{d}\omega_i e^{-i\omega_i t}\int \mathrm{d}\omega_s e^{-i\omega_s t'} e^{-(\omega_s+\omega_i-\bar{\omega}_p)^2/2\sigma_p^2} \\ &\times \mathrm{sinc}\left[\frac{\omega_s-\bar{\omega}_s}{2}T_s + \frac{\omega_i-\bar{\omega}_i}{2}T_i\right] \end{aligned} \tag{5}$$

Equation (5) may be used to obtain a frequency-dispersed signal by eliminating one of the frequency integrations. In Equation (4), we omit the integration over the probe-frequency (ω_r) corresponding to the interaction with $\hat{E}_i$ at time t_4. The same approach is used below to obtain the frequency-dispersed signals.

The GSB diagram shown in Figure 1b(left) is divided into the light-matter interaction and the detection parts. In the former, each arrow represents an interaction of a photon with the molecular sample. Arrows with the same color belong to the same EPP. In the detection part, each arrow represents the interaction of a photon with the detector. Two blue (pink) arrows on opposite branches represent the detection of the i(s)-photon.

We next turn to the ESE signal obtained using Equation (1) with $n_i = 2$ and $n_s = 0$. By calculating Equation (1) together with Equation (3) using time-dependent perturbation theory, we obtain the following expression for the signal,

$$\begin{aligned} S_{QL,ESE}(\tau_1,\tau_2) = 2\mathcal{N}\Re\int_{t_0}^{\infty}\mathrm{d}t_4\int_{t_0}^{\infty}\mathrm{d}t_3\int_{t_0}^{t_4}\mathrm{d}t_2\int_{t_0}^{t_3}\mathrm{d}t_1 \\ \times\langle\psi_m(t_0)|\,\mu_e(t_1)\mu_\nu^{\dagger}(t_3)\mu_\nu(t_4)\mu_e^{\dagger}(t_2)\,|\psi_m(t_0)\rangle \\ \times\left[\Phi^*(t_1,t_4-\tau_2)\Phi(t_2-\tau_1,t_3-\tau_2)\right. \\ \left.+\Phi^*(t_1-\tau_1,t_4-\tau_2)\Phi(t_2,t_3-\tau_2)\right] \end{aligned} \tag{6}$$

The ESE diagram is shown in Figure 1b(center). Here, the two interactions with the s-photon create a vibrational coherence in

the excited state, which results in the zero-photon count in the D_s detector.

Finally, the ESA signal is computed using time-dependent perturbative expansion of Equation (1) for $n_i = 1$, $n_s = 0$,

$$S_{QL,ESA}(\tau_1,\tau_2) = -2\mathcal{N}\Re\int_{t_0}^{\infty}dt_4\int_{t_0}^{\infty}dt_2\int_{t_0}^{t_4}dt_3\int_{t_0}^{t_3}dt_1\,\langle\psi_m(t_0)|\times\mu_e(t_2)\mu_v(t_4)\mu_v^{\dagger}(t_3)\mu_e^{\dagger}(t_1)\,|\psi_m(t_0)\rangle\,[\Phi^*(t_2-\tau_1,t_4-\tau_2)\Phi(t_3-\tau_2,t_1)+\Phi^*(t_2,t_4-\tau_2)\Phi(t_3-\tau_2,t_1-\tau_1)] \quad (7)$$

The ESA diagram is shown in Figure 1(b,right). Similar to the ESE signal, the *s*-photon interactions create a vibrational coherence in the excited electronic states. However, the probe process now involves the absorption and emission of the *i*-photon. Thus, only a single photon is detected in D_i, with a zero-photon count in D_s.

Pathway selectivity in a four-wave mixing technique results in disconnected pathways on top of the selectively probed pathway.[30] These pathways must be taken into account since they can contain signals that are non-trivial to filter. However, in 2DEVS, the disconnected pathways are fewer compared to single-color spectroscopic methods. The disconnected pathways contributing to 2DEVS contain products of two components: One part is independent of the *s*- and the *i*-photon delays, while the other depends on the delay τ_1. The part independent of the delays can be treated as a constant background. Thus, one can construct a linear signal using *s*-photons and subtract its product with the aforementioned constant background from the 2DEVS spectra that contain contributions from the disconnected pathways. A detailed discussion can be found in the Supporting Information along with signal derivations for pathway selectivity in four-wave mixing.

Using Equation 5, we construct 2D frequency-dispersed spectra,

$$S'_{QL}(\omega_r,\omega_1;\tau_2) = \left|\mathcal{F}[S_{QL}(\omega_r,\tau_1;\tau_2)]\right| \quad (8)$$

where $\mathcal{F}$ represents the Fourier transform with respect to the delay τ_1, and the delay τ_2 is treated as a parameter. In a similar manner, 2D frequency-dispersed spectra can be displayed vs τ_1,

$$S''_{QL}(\omega_r,\omega_2;\tau_1) = \left|\mathcal{F}[S_{QL}(\omega_r,\tau_2;\tau_1)]\right| \quad (9)$$

Note that detecting single-photon counts in the far-IR region can be challenging due to the photons being in the same frequency regime as the thermal light. One can use photons in the mid-IR or near-IR frequency regimes in 2DEVS to avoid dealing with the thermal light background. Over the past years, efforts have been made to develop detectors that allow single-photon detection of mid-IR photons, and devices such as photovoltaic detectors, and detectors consisting of superconducting nanowires can be utilized.[47]

3. Results and Discussion

Figure 2 compares the 2D frequency-dispersed signals vs ω_r and ω_2 (see Equation 9) for EPPs and classical pulses. Panels (a–c) show the photon-number resolved measurements of EPPs, while panels (d–f) show the corresponding classical pulse spectra. The GSB contribution to the 2DEVS for EPPs shown in Figure 2a was calculated using Equation (2) and Equation (9) for $\bar{\omega}_s = 3.32$ eV, and $\bar{\omega}_i = 0.32$ eV, with the pump bandwidth being $\sigma_p = 0.06$ eV, while the delays between the entangled photons and the pump pulse are $T_s = 30$ fs, $T_i = -30$ fs. The delay τ_1 is set to be 0 fs in our calculations since it only introduces an overall phase to the signal. Peaks in the 2DEVS spectra are assigned to population and coherence contributions marked by colored circles. Peaks connected via orange-dashed line correspond to the same vibrational state, while those connected via the black-dashed line represent coherence contributions. Two types of peaks appear in the spectra corresponding to vibrational populations, P_j, and to vibrational coherences, C_{ij}, with i and j denoting vibrational states. The former appear around $\omega_2 = 0$ eV, while the latter show up at finite ω_2 values. The strongest peak in Figure 2a at $\omega_r = 0.32$ eV and $\omega_2 = 0$ eV corresponds to the population of the lowest vibration state in the ground electronic state. The spectrum has a mirror symmetry around $\omega_2 = 0$ eV. The weaker peaks at $\omega_2 = 0.1$ eV and $\omega_2 = -0.1$ eV represent the coherence between two vibrational states separated by 0.1 eV. The signal intensity is normalized with respect to the peak intensity for the ESA contribution of the signal, as shown in Figure 2c.

Figure 2b depicts the ESE contribution calculated using Equation (6) and Equation (9). The strongest $\omega_r = 0.32$ eV peak represents vibrational population, P_3, in the excited electronic state. The other population peak appears at $\omega_r = 0.16$ eV, and corresponds to the vibrational population P_4. The vibration population peaks in 2DEVS spectra are connected by a red-dashed line. The vibrational coherence peaks appear at $\omega_2 = 0.16$ eV, which corresponds to the vibrational frequency in the excited electronic state.

ESA peaks shown in Figure 2c appear in a similar fashion to the ESE. The three peaks at $\omega_2 = 0$ eV connected by the red-dashed line represent vibrational populations in the excited electronic state. The coherence peaks at $\omega_2 = 0.16$ eV are connected by the black-dashed line. The key difference between the ESE and ESA stems from the nature of the probe of the vibrational coherence created by the first two interactions. The ESE contribution involves the stimulated emission of *i*-photons, and hence cannot have contributions from the lowest vibrational state in the excited electronic state. The probe process in the ESA is of Raman type, and hence does not detect the population and coherence contributions from the highest vibrational state in the excited electronic state.

Comparison of quantum signals with 2DEVS spectra obtained by classical pulses reveals the role of the photon-entanglement. The first two pulses that induce vibronic transitions have the center-frequency of 3.32 eV, whereas the probe pulse has a center-frequency of 0.32 eV. All the pulses have a $\sigma_p = 0.06$ eV bandwidth. The GSB, ESE, and ESA contributions to the classical 2DEVS signal are shown in Figure 2d–f. These contributions may not be separated by classical experiments but can be revealed by EPP spectra. In the GSB contribution (see Figure 2d), the strong peak at $\omega_2 = 0$ eV corresponds to the vibrational population in the ground electronic state. Sidebands corresponding to vibrational coherence appear at $\omega_2 = 0.1$ eV (and –0.1 eV), but unlike the EPPs signals, the peaks are not resolved along the probe-frequency axis.

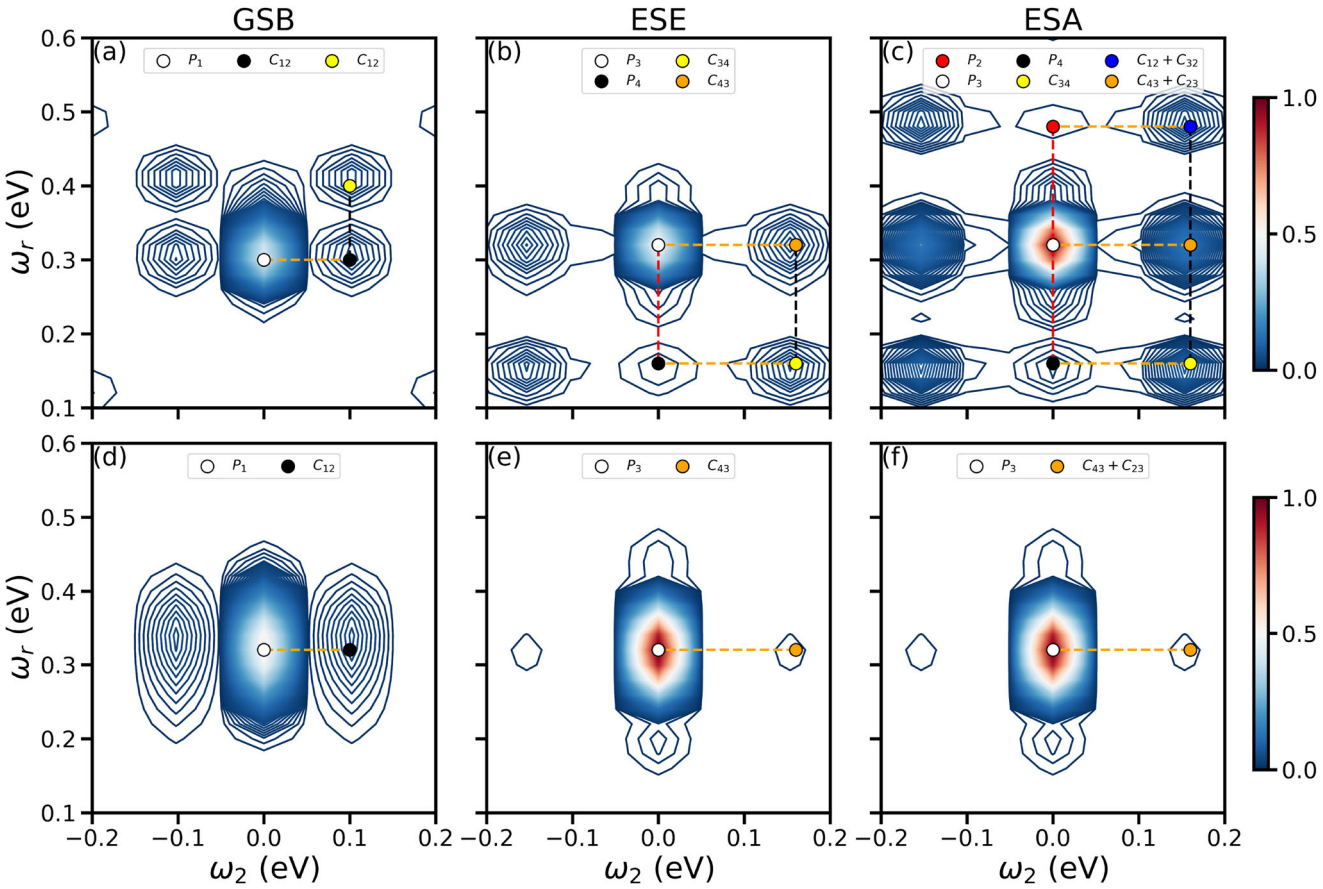

Figure 2. 2D frequency-dispersed (ω_r, ω_2) spectra for quantum and classical light calculated using Equation (9). a–c) GSB, ESE, and ESA contributions to the 2DEVS signals for the model system under study, respectively. d–f) GSB, ESE, and ESA contributions to 2DEVS signals, respectively, constructed using classical pulses. Vibrational population (P_j) and coherence (C_{ij}) peaks are marked in the spectra, where i and j represent vibrational states. Population (coherent) peaks are connected via a red (black)-dashed line. The population and coherence peaks connected via an orange-dashed line stem from the same vibrational level. The spectra are calculated for the delay $\tau_1 = 0$ fs. Quantum light parameters: $\sigma_p = 0.06$ eV, $T_s = 30$ fs, $T_i = -30$ fs, $\omega_p = 3.64$ eV, $\omega_s = 3.32$ eV, and $\omega_i = 0.32$ eV. Classical spectra are constructed using pulses with $\sigma_p = 0.06$ eV spectral width.

A more pronounced photon entanglement effect appears in the ESE and ESA spectra, where the participating vibrational states have a 0.16 eV frequency. The classical ESE and ESA contributions shown in Figure 2e,f, respectively, only contain two vibrational coherence peaks along with a single population peak, which carries considerably less information compared to the EPP spectra. Entangled-photon 2DEVS thus provides as improved probe of vibrational excitations due to an increase in the bandwidth of the photons owing to the entanglement time. However, entangled photons are just a convenient source to achieve the discussed pathway selectivity along with an improved spectral resolution, and similar results can be obtained by using classical pulses with a larger bandwidth. Additionally, ESE and ESA contributions to the classical signal are very similar but with opposite signs, as evident by the signal expression (Equation S10 and S12) in the Supporting Information. The two contributions thus cancel out, and the GSB dominates the signal. A classical 2DEVS signal cannot probe vibrational dynamics in an excited electronic state when the three contributions spectrally overlap.

To demonstrate the effect of the entanglement time ($T_e = T_s$-T_i) on the 2DEVS spectra, **Figure 3**a–c shows the ESA spectra constructed using Equation (7) and Equation (9) for several entanglement times $T_e = 40$ fs ($T_s = 10$ fs. $T_i = -30$ fs), $T_e = 60$ fs ($T_s = 30$ fs. $T_i = -30$ fs), and $T_e = 40$ fs ($T_s = 30$ fs. $T_i = -10$ fs), respectively. Three population peaks appear for $T_e = 40$ fs, as shown in Figure 3a. These peaks appear at $\omega_2 = 0$ eV for the probe frequencies $\omega_r = 0.16$, 0.32, and 0.48 eV. Coherence peaks appear at two finite ω_2 values: 0.16, and 0.32 eV. A single coherence peak appears for $\omega_r = 0.32$ eV, while two coherence peaks appear for $\omega_r = 0.16$ eV and $\omega_r = 0.48$ eV. The number of coherence peaks decreases with an increase in ω_2. Similar features appear in the signal shown in Figure 3c for the same entanglement time of $T_e = 40$ fs, but for different signal and idler delays. In contrast, the ESA signal for the entanglement time of $T_e = 60$ fs shows distinct features from $T_e = 40$ fs. For example, the coherence and population features are stronger than the central peak at $\omega_r = 0.32$ eV and $\omega_2 = 0$ eV in the ESA signal with $T_e = 40$ fs. Additionally, an extra coherence peak appears in Figure 3b compared to Figure 3a, represented by the magenta circle at $\omega_r = \omega_2 = 0.32$ eV. The emergence of distinct coherence features in the spectra for two entanglement times stems from the change in the TPA of the EPPs with the entanglement time along with T_s and T_i. Figure 3d shows the TPA

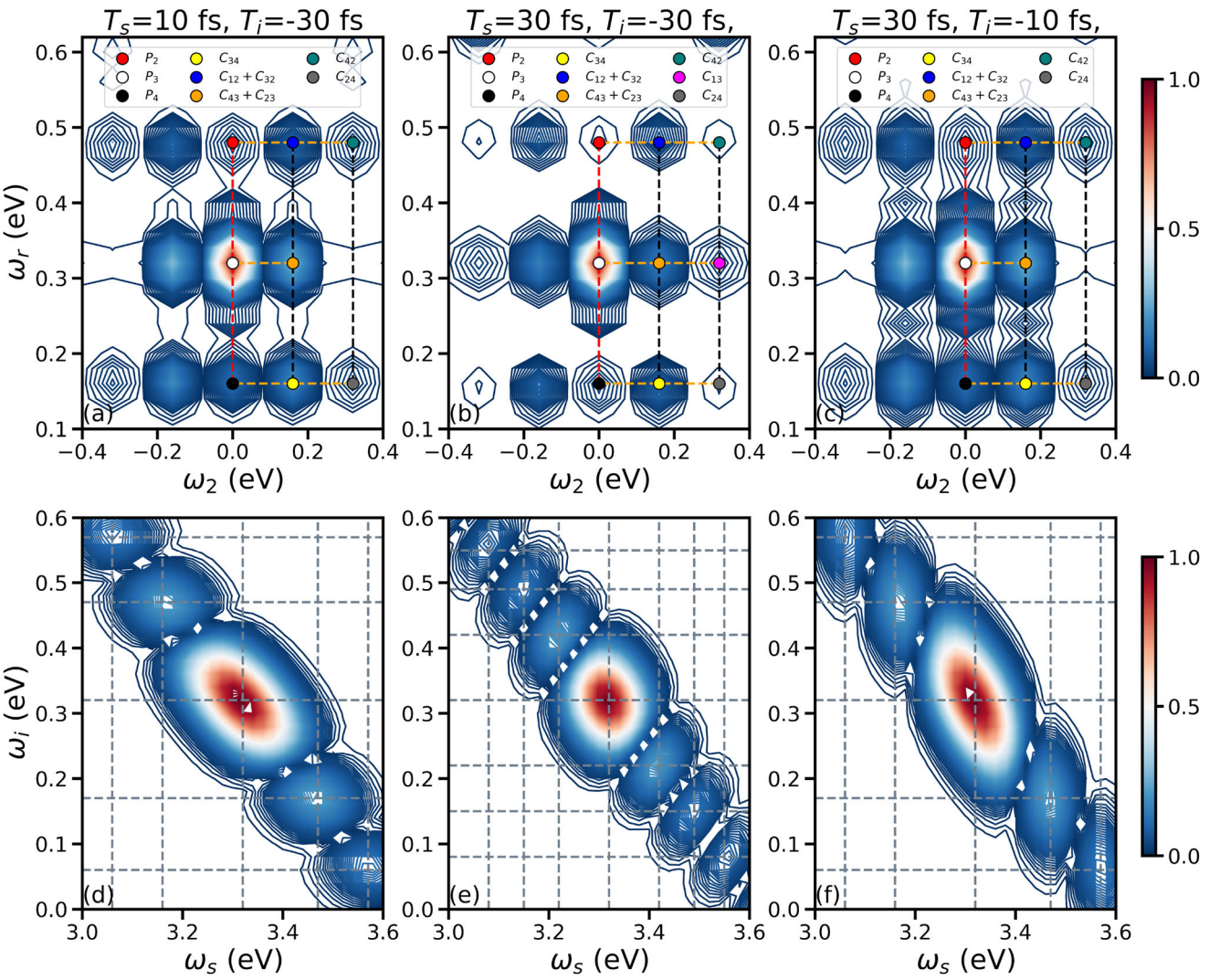

Figure 3. 2D frequency-dispersed ESA spectra for different entanglement times calculated using Equation (9). a–c) Spectra dispersed over ω_r and ω_2 are shown for T_e = 40 fs (T_s = 10 fs. T_i = –30 fs), T_e = 60 fs (T_s = 30 fs. T_i = -30 fs), and T_e = 40 fs (T_s = 30 fs. T_i = -10 fs), respectively. Peaks at ω_2 = 0 eV represent vibrational population contributions, and peaks at non-zero ω_2 represent vibrational coherence contributions. d–f) TPAs dispersed over ω_s and ω_i are shown corresponding to EPPs used in (a), (b), and (c), respectively. Quantum light parameters: σ_p = 0.06 eV, ω_p = 3.64 eV, ω_s = 3.32 eV, and ω_i = 0.32 eV.

for the entanglement time of T_e = 40 fs with T_s = 10 fs and T_i = –30 fs. The number of islands that represent the TPA for signal and idler frequencies, ω_s and ω_i, respectively, is lower than for the entanglement time T_e = 60 fs shown in Figure 3e. Additionally, the positions of the islands in the two TPAs are different, as can be seen by vertical and horizontal intersecting lines along the anti-diagonal. This leads to different molecular transitions that are accessible for the two entanglement times.

Figure 3a,c shows similar features due to the same entanglement time, even though the signal and idler-photon delays are different. Interestingly, the islands in TPA for the same entanglement time of T_e = 40 fs with different T_s and T_i values appear at exactly the same signal and idler frequencies, as can be seen in Figure 3d,f. Changing the entangled photon delays while holding the entanglement time fixed changes the shapes of the islands in TPA without affecting their position along signal and idler frequencies. Increasing the delay of the s (i)-photon, T_s (T_i), reduces the TPA along the s (i)-photon frequency axis. This helps control the resolutions provided by the signal and idler photons in the signal.

To further study the impact of signal and idler delays on 2DEVS spectra, we have examined 2D frequency-dispersed ESA spectra in ω_r/ω_1 space. **Figure 4** shows the 2D frequency-dispersed signals around ω_r and ω_1 constructed using Equation (7) and Equation (8). The ESA signals for the signal and idler delays T_s = 10 fs, T_i = -60 fs, and T_s = 60 fs, T_i = -10 fs are shown in Figure 4a and Figure 4b, respectively. Note that both spectra are constructed for the same entanglement time of T_e = 70 fs. Peaks that appear in the 2DEVS spectra have contributions from both vibrational populations and coherences. The ω_r = 0.32 eV and ω_1 = 3.32 eV peak has the maximum intensity in both spectra since the idler and signal photons have center frequencies of

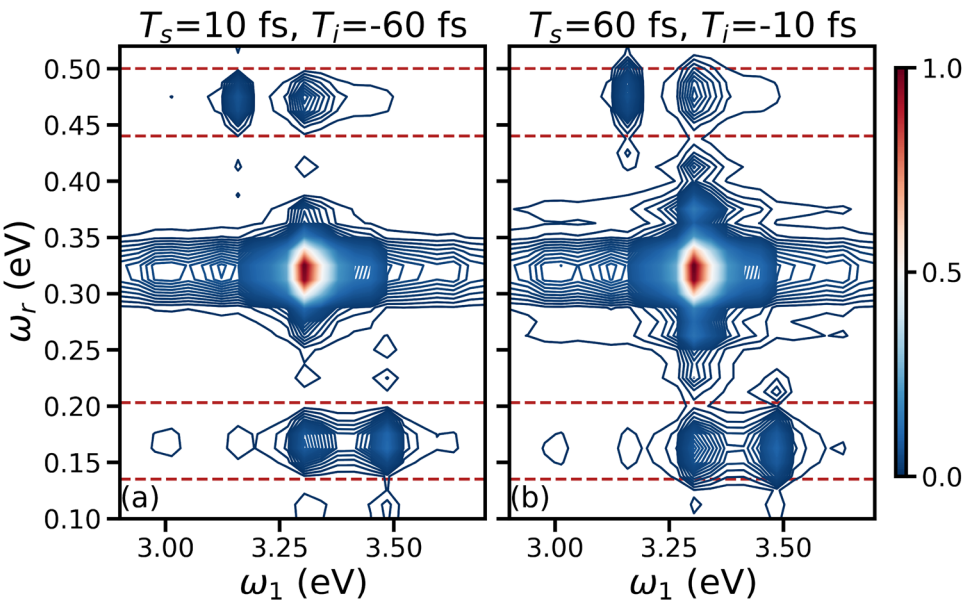

Figure 4. 2D frequency-dispersed ESA spectra for different entanglement times using Equation (8). Spectra dispersed over ω_r and ω_1 are shown here for a) T_s = 10 fs, T_i = -60 fs, and for b) T_s = 60 fs, T_i = -10 fs with $\tau_2 - \tau_1$ = 280 fs. Red-dashed lines are drawn to show the width of peaks in the panel (a) and compare it with the widths of peaks in the panel (b). Quantum light parameters: σ_p = 0.06 eV, ω_p = 3.64 eV, ω_s = 3.32 eV, and ω_i = 0.32 eV.

0.32 and 3.32 eV, respectively. The signal centered at $\omega_r = 0.32$ eV and $\omega_1 = 3.32$ eV has a larger bandwidth in Figure 4a compared to Figure 4b along ω_r. The peaks at $\omega_r = 0.16$ eV, and 0.48 eV in Figure 4b are broader compared to the corresponding peaks in Figure 4a, as can be seen with the help of horizontal-dashed lines. The lines are drawn such that they entirely contain the peaks at $\omega_r = 0.16$ eV, and 0.48 eV in Figure 4a. When the lines are drawn at the same ω_r frequencies in Figure 4b, the peaks cross the lines on either or both sides, indicating the increased bandwidth of the peaks along ω_r.

4. Conclusion

We have proposed a quantum setup that can select different Liouville pathways in 2DEVS four-wave mixing using visible and infrared entangled photons. The GSB, ESE, and ESA contributions can be isolated through the number of photons detected in coincidence. This pathway discrimination allows for a separate study of molecular vibrational dynamics in the ground and excited states. Photon entanglement has been used to construct 2DEVS spectra that contain more features compared to classical signals for a given pulse bandwidth. The entanglement between the two photons can be tuned in order to access a broader range of vibronic transitions. The photon entanglement-time plays an important role as well, and changing the entanglement time gives access to different vibronic transitions due to the change in the TPA. In addition, changing the signal and idler photon delays without changing the entanglement time allows controlling the spectral resolution provided by the two photons.

Supporting Information

Supporting Information is available from the Wiley Online Library or from the author.

Acknowledgements

U.H. acknowledges support from the Science and Engineering Board, India, under Grant No. CRG/2020/0011100 and the Fulbright-Nehru Academic and Excellence Fellowship (India), 2023-24. M.K. acknowledges the support from the Alexander von Humboldt Foundation through the Feodor Lynen program. V.Y.C. and S.M. gratefully acknowledge the support of the US Department of Energy, Office of Science, Basic Energy Sciences Award DES0022134, which has primarily funded this work. S.M. gratefully acknowledges the support of the National Science Foundation through Grant No. CHE-2246379. S.M. gratefully acknowledges support from the Department of Energy through Grant no. DE-SC0023233.

Conflict of Interest

The authors declare no conflicts of interest.

Data Availability Statement

The data that support the findings of this study are available from the corresponding author upon reasonable request.

Keywords

2D spectroscopy, electronic-vibrational spectroscopy, entangled photons

Received: September 24, 2024
Revised: December 17, 2024
Published online:

[1] Y. Shih, *IEEE J. Sel. Top. Quant.* **2003**, *9*, 1455.
[2] A. Eshun, O. Varnavski, J. P. Villabona-Monsalve, R. K. Burdick, T. Goodson III, *Accounts Chem. Res.* **2022**, *55*, 991.

[3] K. E. Dorfman, F. Schlawin, S. Mukamel, *Rev. Mod. Phys.* **2016**, *88*, 045008.
[4] F. Schlawin, *J. Phys. B: At. Mol. Opt.* **2017**, *50*, 203001.
[5] N. P. Georgiades, E. Polzik, K. Edamatsu, H. Kimble, A. Parkins, *Phys. Rev. Lett.* **1995**, *75*, 3426.
[6] D.-I. Lee, T. Goodson, *J. Phys. Chem. B* **2006**, *110*, 25582.
[7] B. Dayan, A. Pe'Er, A. A. Friesem, Y. Silberberg, *Phys. Rev. Lett.* **2004**, *93*, 023005.
[8] H.-B. Fei, B. M. Jost, S. Popescu, B. E. Saleh, M. C. Teich, *Phys. Rev. Lett.* **1997**, *78*, 1679.
[9] V. Giovannetti, S. Lloyd, L. Maccone, *Sci. J.* **2004**, *306*, 1330.
[10] S. Mukamel, M. Freyberger, W. Schleich, M. Bellini, A. Zavatta, G. Leuchs, C. Silberhorn, R. W. Boyd, L. L. Sánchez-Soto, A. Stefanov, et al., *J. Phys. B: At. Mol. Opt.* **2020**, *53*, 072002.
[11] K. E. Dorfman, F. Schlawin, S. Mukamel, *J Phys. Chem. Lett.* **2014**, *5*, 2843.
[12] F. Schlawin, S. Mukamel, *J. Chem. Phys.* **2013**, *139*, 24.
[13] F. Schlawin, K. E. Dorfman, B. P. Fingerhut, S. Mukamel, *Nat. Comm.* **2013**, *4*, 1782.
[14] F. Chen, B. Gu, S. Mukamel, *ACS Photonics* **2022**, *9*, 1889.
[15] B. Gu, S. Sun, F. Chen, S. Mukamel, *Proc. Nat. Acad. Sci.* **2023**, *120*, e2300541120.
[16] D. Jadoun, Z. Zhang, M. Kowalewski, *J. Phys. Chem. Lett.* **2024**, *15*, 2023.
[17] L. Ko, R. L. Cook, K. B. Whaley, *J. Phys. Chem. Lett.* **2023**, *14*, 8050.
[18] H. Gebbie, R. Twiss, *Rep. Prog. Phys.* **1966**, *29*, 729.
[19] O. Roslyak, C. A. Marx, S. Mukamel, *Phys. Rev. A* **2009**, *79*, 033832.
[20] M. G. Raymer, A. H. Marcus, J. R. Widom, D. L. Vitullo, *J. Phys. Chem. B* **2013**, *117*, 15559.
[21] J. Lavoie, T. Landes, A. Tamimi, B. J. Smith, A. H. Marcus, M. G. Raymer, *Adv. Quantum Tech.* **2020**, *3*, 1900114.
[22] Y. Fujihashi, A. Ishizaki, R. Shimizu, *J. Chem. Phys.* **2024**, *160*, 10.
[23] M. Kizmann, H. K. Yadalam, V. Y. Chernyak, S. Mukamel, *Proc. Nat. Acad. Sci.* **2023**, *120*, e2304737120.
[24] H. K. Yadalam, M. Kizmann, J. R. Rouxel, Y. Nam, V. Y. Chernyak, S. Mukamel, *J. Phys. Chem. Lett.* **2023**, *14*, 10803.
[25] S. Mukamel, *Principles of nonlinear optical spectroscopy*, Oxford University Press, **1995**.
[26] S. Asban, S. Mukamel, *Sci. Adv.* **2021**, *7*, eabj4566.
[27] S. Asban, V. Y. Chernyak, S. Mukamel, *J. Chem. Phys.* **2022**, *156*, 9.
[28] L. Ye, S. Mukamel, *Appl. Phys. Lett.* **2020**, *116*, 17.
[29] Y. Fujihashi, A. Ishizaki, *J. Chem. Phys.* **2021**, *155*, 4.
[30] H. K. Yadalam, M. Kizmann, S. Mukamel, *Optica Quantum* **2024**, *2*, 330.
[31] T. A. Oliver, N. H. Lewis, G. R. Fleming, *Proc. Nat. Acad. Sci.* **2014**, *111*, 10061.
[32] N. H. Lewis, G. R. Fleming, *J. Phys. Chem. Lett.* **2016**, *7*, 831.
[33] E. A. Arsenault, P. Bhattacharyya, Y. Yoneda, G. R. Fleming, *J. Chem. Phys.* **2021**, *155*, 2.
[34] A. R. Grossman, D. Bhaya, K. E. Apt, D. M. Kehoe, *Annu. Rev. Genet.* **1995**, *29*, 231.
[35] Z. Liu, H. Yan, K. Wang, T. Kuang, J. Zhang, L. Gui, X. An, W. Chang, *Nature* **2004**, *428*, 287.
[36] G. McDermott, S. Prince, A. Freer, A. Hawthornthwaite-Lawless, M. Papiz, R. Cogdell, N. Isaacs, *Nature* **1995**, *374*, 517.
[37] T. L. Courtney, Z. W. Fox, K. M. Slenkamp, M. Khalil, *J. Chem. Phys.* **2015**, *143*, 15.
[38] N. H. Lewis, N. L. Gruenke, T. A. Oliver, M. Ballottari, R. Bassi, G. R. Fleming, *J. Phys. Chem. Lett.* **2016**, *7*, 4197.
[39] E. C. Wu, E. A. Arsenault, P. Bhattacharyya, N. H. Lewis, G. R. Fleming, *Faraday Discuss.* **2019**, *216*, 116.
[40] E. A. Arsenault, Y. Yoneda, M. Iwai, K. K. Niyogi, G. R. Fleming, *Nat. Comm.* **2020**, *11*, 1460.
[41] E. A. Arsenault, Y. Yoneda, M. Iwai, K. K. Niyogi, G. R. Fleming, *Nat. Comm.* **2020**, *11*, 6011.
[42] J. D. Gaynor, M. Khalil, *J. Chem. Phys.* **2017**, *147*, 9.
[43] J. D. Gaynor, A. Petrone, X. Li, M. Khalil, *J. Phys. Chem. Lett.* **2018**, *9*, 6289.
[44] E. A. Arsenault, A. J. Schile, D. T. Limmer, G. R. Fleming, *J. Chem. Phys.* **2021**, *155*, 5.
[45] P. Kelley, W. Kleiner, *Phys. Rev.* **1964**, *136*, A316.
[46] R. Scholz, G. Friege, K.-A. Weber, *Eur. J. Physics* **2018**, *39*, 055301.
[47] S. Dello Russo, A. Elefante, D. Dequal, D. K. Pallotti, L. Santamaria Amato, F. Sgobba, M. Siciliani de Cumis, in *Photonics*, vol. *9*, MDPI, **2022**, pp. 470.

LASER
& PHOTONICS
REVIEWS

Supporting Information

for *Laser Photonics Rev.*, DOI 10.1002/lpor.202401576

Pathway Selectivity in 2D Electronic-Vibrational Spectroscopy with Quantum Light

Deependra Jadoun, Hari K. Yadalam, Upendra Harbola, Vladimir Y. Chernyak, Matthias Kizmann and Shaul Mukamel**

Supplementary Information: Pathway Selectivity in Two-Dimensional Electronic-Vibrational Spectroscopy with Quantum Light

Deependra Jadoun,[†,‡] Hari K. Yadalam,[†,‡] Upendra Harbola,[¶] Vladimir Y. Chernyak,[§,‖] Matthias Kizmann,[*,†,‡] and Shaul Mukamel[*,†,‡]

†*Department of Chemistry, University of California, Irvine, CA 92614, USA*

‡*Department of Physics and Astronomy, University of California, Irvine, CA 92614, USA*

¶*Department of Inorganic and Physical Chemistry, Indian Institute of Science, Bangalore 560012, India*

§*Department of Chemistry, Wayne State University, 5101 Cass Ave, Detroit, Michigan 48202, USA*

‖*Department of Mathematics, Wayne State University, 656 W. Kirby, Detroit, Michigan 48202, USA*

E-mail: matthias.kizmann@web.de; smukamel@uci.edu

The Model System

Figure S1 shows the vibronic energy levels of the model system used in our study. For the used model system, the total Hamiltonian is given by,

$$\hat{H} = \hat{H}_F + \hat{H}_M + \hat{H}_{int} \tag{S1}$$

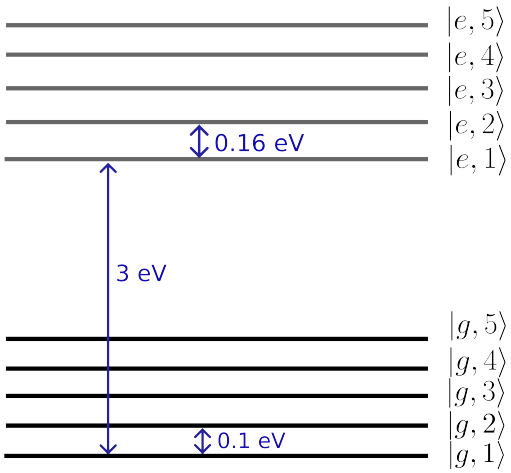

Figure S1: Energy levels in the model system are shown. Two electronic states ($|g\rangle$ and $|e\rangle$) with five vibrational states each are considered in the model system. The ground state $|g\rangle$ and the excited state $|e\rangle$ vibrational frequencies are 0.1 eV and 0.16 eV, respectively.

where $\hat{H}_F = \sum_{j=1}^{4} \int \mathrm{d}\omega_j \hbar \hat{a}_j^\dagger \hat{a}_j$ represents the Field Hamiltonian with $\hat{a}_j$ ($\hat{a}_j^\dagger$) being the photon annihilation (creation) operator for four fields that interact with the molecules. $\hat{H}_M$ represents the matter Hamiltonian expressed as follows,

$$\hat{H}_M = \sum_{\sigma=e,g} \sum_{n=1}^{5} \hbar\omega_{\sigma,n} \left|\sigma, n\right\rangle \left\langle\sigma, n\right| \tag{S2}$$

where $\omega_{\sigma,n}$ represents the energy of the vibrational state $n \in (1,5)$ in the electronic state $\sigma \in \{g, e\}$, with g and e representing ground and excited electronic states. The light-matter interaction Hamiltonian $\hat{H}_{int}$ is expressed as follows,

$$\hat{H}_{int} = \sum_{n,n'=1}^{5} \sum_{j=1,2} \left|e_n\right\rangle \left\langle g_{n'}\right| \hat{\mu}_{en,gn'} \hat{E}_j + \sum_{n,n'=1}^{5} \sum_{\sigma=e,g} \sum_{j'=3,4} \left|\sigma_n\right\rangle \left\langle\sigma_{n'}\right| \hat{\mu}_{\sigma n,\sigma n'} \hat{E}_{j'} + \text{h.c.} \tag{S3}$$

where $\hat{\mu}_\sigma n, \sigma n'$ represents the transition dipole moment (TDM) operator for the transitions between vibronic levels σ_n and σ'_n, and $\hat{E}_j$ ($\hat{E}_{j'}$) represents the electric field operator for the pulse in ultraviolet (UV)/visible (infrared (IR)) energy regime that is responsible for

vibronic (vibrational) transition. The electric field operator can be expressed as follows,

$$\hat{E} = \sum_{j=1}^{4} i\hat{e}_j \mathcal{E}_j \int \mathrm{d}\omega \hat{a}_j(\omega) e^{i\vec{k}_j \cdot \vec{r}} \tag{S4}$$

where $\hat{e}_j$ is the polarization, $\vec{k}_j$ is the wavevector of the photon, $\mathcal{E}_j$ represents the amplitude of the electric field, $\hat{a}_j(\omega)$ is the annihilation operator for the photon j with the mode frequency ω, and $\vec{r}$ is the position vector.

Quantum 2DEV Signals

Ground State Bleach

The ground state bleach contribution is selectively probed by detecting one photon in D_s and one photon in D_i, and the signal is defined as,

$$S_{GSB} = \left\langle \mathbf{T} \Omega_s e^{-\Omega_s} \Omega_i e^{-\Omega_i} \right\rangle \tag{S5}$$

where $\mathbf{T}$ represents the time-ordering, $\Omega_{s/i} = \int \mathrm{d}\tau_{s/i} \hat{E}^{\dagger}_{s/i,R}(\tau_{s/i}) \hat{E}_{s/i,L}(\tau_{s/i})$, which leads to the following expression,

$$S_{GSB} = \int \mathrm{d}\tau_i \int \mathrm{d}\tau_s \left\langle \mathbf{T} \hat{E}^{\dagger}_{i,R}(\tau_i) \hat{E}_{i,L}(\tau_i) \hat{E}^{\dagger}_{s,R}(\tau_s) \hat{E}_{s,L}(\tau_s) \rho(t) \right\rangle \tag{S6}$$

where $\rho(t) = \rho_F(t)\rho_M(t)$ is the total density matrix at time t with ρ_F and ρ_M being density matrices for field and matter, respectively. Using the perturbative expansion of the total

density matrix up to the fourth order leads to the following signal expression,

$$
\begin{aligned}
S_{GSB} =& \frac{2}{\hbar^4}\Re \int \mathrm{d}\tau_s \int \mathrm{d}\tau_i \Bigg[\int_{-\infty}^{\infty} \mathrm{d}t_4 \int_{-\infty}^{t_4} \mathrm{d}t_3 \int_{-\infty}^{t_3} \mathrm{d}t_2 \int_{-\infty}^{t_2} \mathrm{d}t_1 \left\langle \psi_M \right| \hat{\mu}_4(t_4)\hat{\mu}_2^{\dagger}(t_3)\hat{\mu}_2(t_2)\hat{\mu}_1^{\dagger}(t_1) \left| \psi_M \right\rangle \\
& \times \left\langle \psi_F \right| \hat{E}_s^{\dagger}(\tau_s)\hat{E}_i^{\dagger}(\tau_i)\hat{E}_s(\tau_s)\hat{E}_i(\tau_i)\hat{E}_4^{\dagger}(t_4)\hat{E}_3(t_3)\hat{E}_2^{\dagger}(t_2)\hat{E}_1(t_1) \left| \psi_F \right\rangle + \\
& \int_{-\infty}^{\infty} \mathrm{d}t_4 \int_{-\infty}^{t_4} \mathrm{d}t_3 \int_{-\infty}^{\infty} \mathrm{d}t_2 \int_{-\infty}^{t_2} \mathrm{d}t_1 \left\langle \psi_M \right| \hat{\mu}_1(t_1)\hat{\mu}_2^{\dagger}(t_2)\hat{\mu}_4(t_4)\hat{\mu}_3^{\dagger}(t_3) \left| \psi_M \right\rangle \\
& \times \left\langle \psi_F \right| \hat{E}_1^{\dagger}(t_1)\hat{E}_2(t_2)\hat{E}_s^{\dagger}(\tau_s)\hat{E}_i^{\dagger}(\tau_i)\hat{E}_i(\tau_i)\hat{E}_s(\tau_s)\hat{E}_4^{\dagger}(t_4)\hat{E}_3(t_3) \left| \psi_F \right\rangle \Bigg]
\end{aligned}
\tag{S7}
$$

Note that here we derive the signal for generic four-wave mixing with different electric field notations, and we will transform the expression to two-dimensional electronic-vibrational spectroscopy (2DEVS) in the final step. The field correlation functions can be simplified by integrating over τ_s and τ_i, and the final expression reads,

$$
\begin{aligned}
S_{GSB} =& \frac{2}{\hbar^4}\Re \Bigg[\int_{-\infty}^{\infty} \mathrm{d}t_4 \int_{-\infty}^{t_4} \mathrm{d}t_3 \int_{-\infty}^{t_3} \mathrm{d}t_2 \int_{-\infty}^{t_2} \mathrm{d}t_1 \left\langle \psi_M \right| \hat{\mu}_4(t_4)\hat{\mu}_3^{\dagger}(t_3)\hat{\mu}_2(t_2)\hat{\mu}_1^{\dagger}(t_1) \left| \psi_M \right\rangle \\
& \times \left\langle \psi_F \right| \hat{E}_2^{\dagger}(t_2)\hat{E}_4^{\dagger}(t_4)\hat{E}_3(t_3)\hat{E}_1(t_1) \left| \psi_F \right\rangle \\
& + \int_{-\infty}^{\infty} \mathrm{d}t_4 \int_{-\infty}^{t_4} \mathrm{d}t_3 \int_{-\infty}^{\infty} \mathrm{d}t_2 \int_{-\infty}^{t_2} \mathrm{d}t_1 \left\langle \psi_M \right| \hat{\mu}_1(t_1)\hat{\mu}_2^{\dagger}(t_2)\hat{\mu}_4(t_4)\hat{\mu}_3^{\dagger}(t_3) \left| \psi_M \right\rangle \\
& \times \left\langle \psi_F \right| \hat{E}_1^{\dagger}(t_1)\hat{E}_4^{\dagger}(t_4)\hat{E}_3(t_3)\hat{E}_2(t_2) \left| \psi_F \right\rangle \Bigg]
\end{aligned}
\tag{S8}
$$

The expression in the main text is customized for 2DEVS, where field operators with delay T_2 correspond to the i-photon, while the remaining field operators correspond to the s-photon. A multi-dimensional time-grid is used to represent the four-point correlation functions corresponding to each pathway in 2DEVS. Integrations over the four time variables are calculated numerically following the multiplication of the matter correlation function with the entangled field amplitudes.

Four-point matter correlation functions in the above expressions can be visualized us-

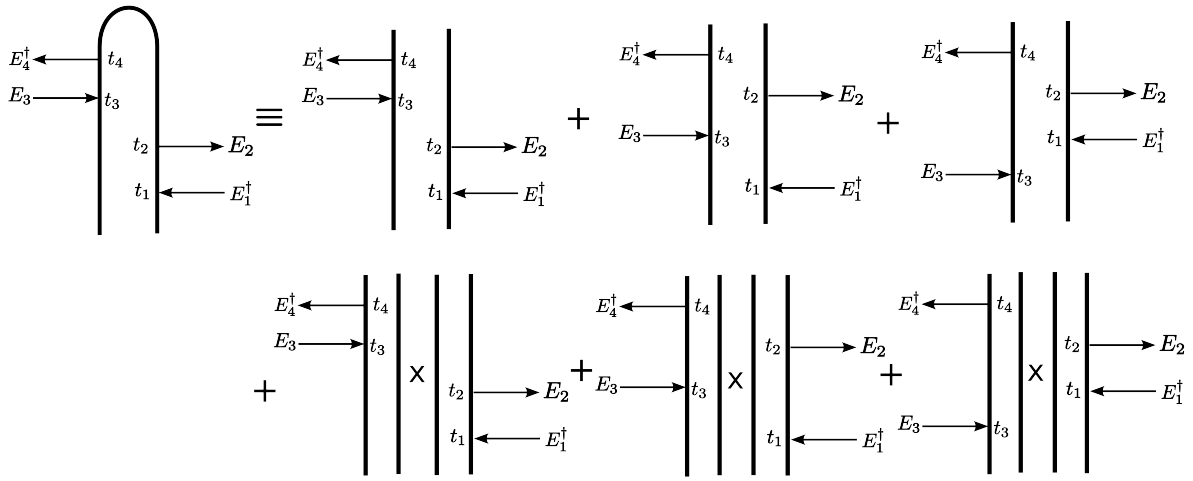

Figure S2: Ladder diagrams corresponding to a loop diagram for ground state bleach (GSB). Top row shows complete diagrams, while the bottom row shows disconnected diagrams.

ing loop diagrams. Figure S2 shows a loop diagram forground state bleach (GSB) along with corresponding complete and disconnected ladder diagrams. The ladder diagrams in the top row represent complete contributions, whereas the diagrams in the bottom row are disconnected contributions. Note that the right two ladder diagrams do not represent GSB contribution and are still part of the loop diagram. To consider only the true GSB contribution in 2DEVS, the delay of the i-photon can be set much larger than the pulse width, which eliminates the non-GSB contributions. In principle, disconnected parts contribute to the selected pathway, but due to non-degenerate frequencies of the entangled photons in 2DEVS, the disconnected part in our study can be filtered out. Only the part corresponding to $\hat{E}_1$ and $\hat{E}_2$ in the disconnected contributions depends on the delay T_1, while the other part is a constant background. Therefore, a linear signal in the field intensity constructed using $\hat{E}_1$ and $\hat{E}_2$ fields can be used to calculate the disconnected part in GSB that depends on the relative delay between the two pulses, which can be subtracted from the 2DEVS signal.

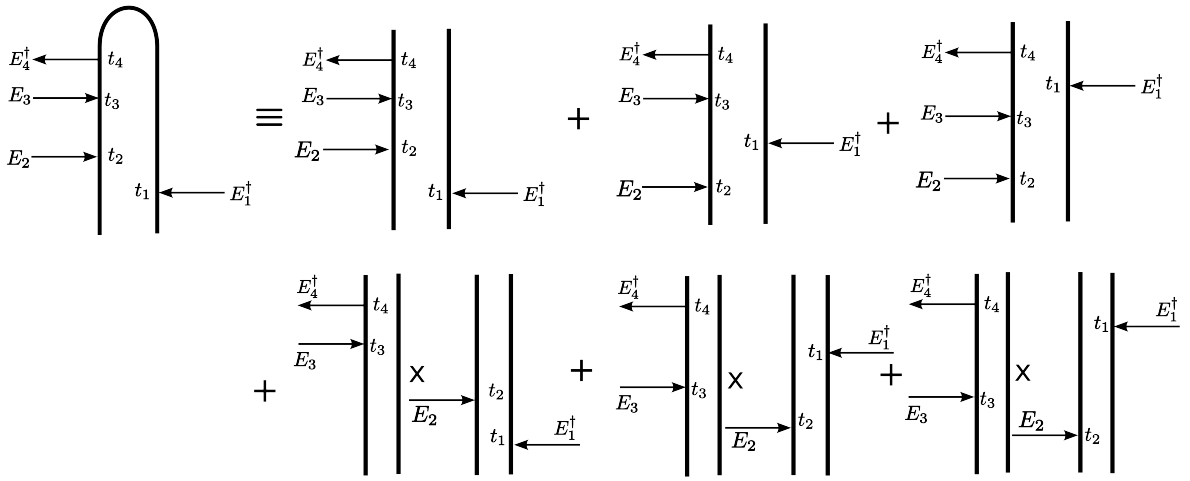

Figure S3: Ladder diagrams corresponding to a loop diagram for excited state absorption (ESA). The top row shows complete diagrams, while the bottom row shows disconnected diagrams.

Excited State Absorption

Excited state absorption (ESA) contribution is probed when one photon is detected in D_i and zero photons in D_s, and the coincidence-count signal is defined as,

$$S_{ESA} = \left\langle \mathbf{T}\Omega_i e^{-\Omega_i} \right\rangle \tag{S9}$$

Following the same steps used to derive the GSB signal, we get the final signal expression for ESA,

$$\begin{aligned} S_{ESA} = -\frac{2}{\hbar^4}\Re\Bigg[& \int_{-\infty}^{\infty} \mathrm{d}t_4 \int_{-\infty}^{t_4} \mathrm{d}t_3 \int_{-\infty}^{\infty} \mathrm{d}t_2 \int_{-\infty}^{t_3} \mathrm{d}t_1 \left\langle \psi_M \right| \hat{\mu}_2(t_2)\hat{\mu}_4(t_4)\hat{\mu}_3^\dagger(t_3)\hat{\mu}_1^\dagger(t_1) \left| \psi_M \right\rangle \\ & \times \left\langle \psi_F \right| \hat{E}_2^\dagger(t_2)\hat{E}_4^\dagger(t_4)\hat{E}_3(t_3)\hat{E}_1(t_1) \left| \psi_F \right\rangle \\ & + \int_{-\infty}^{\infty} \mathrm{d}t_4 \int_{-\infty}^{t_4} \mathrm{d}t_3 \int_{-\infty}^{t_3} \mathrm{d}t_2 \int_{-\infty}^{\infty} \mathrm{d}t_1 \left\langle \psi_M \right| \hat{\mu}_1(t_1)\hat{\mu}_4(t_4)\hat{\mu}_3^\dagger(t_3)\hat{\mu}_2^\dagger(t_2) \left| \psi_M \right\rangle \\ & \times \left\langle \psi_F \right| \hat{E}_1^\dagger(t_1)\hat{E}_4^\dagger(t_4)\hat{E}_3(t_3)\hat{E}_2(t_2) \left| \psi_F \right\rangle \Bigg] \end{aligned} \tag{S10}$$

Figure S3 shows a loop diagram corresponding to ESA signal, along with the contributing

ladder diagrams from complete (top row) and disconnected (bottom row) components. The right-most ladder diagram in the top row does not represent the ESA contribution, and it can be eliminated by setting the delay between the s- and i-photons larger than the pump-width that creates entangled photons. The contribution from the disconnected parts can be treated in ESA contribution in a similar manner as the GSB contribution since only the terms with $\hat{E}_1$ and $\hat{E}_2$ fields depends on the delay τ_1 while the other component is a constant background. One can construct a transient absorption signal using $\hat{E}_1$ and $\hat{E}_2$ fields and subtract from the ESA signal.

Excited State Emission

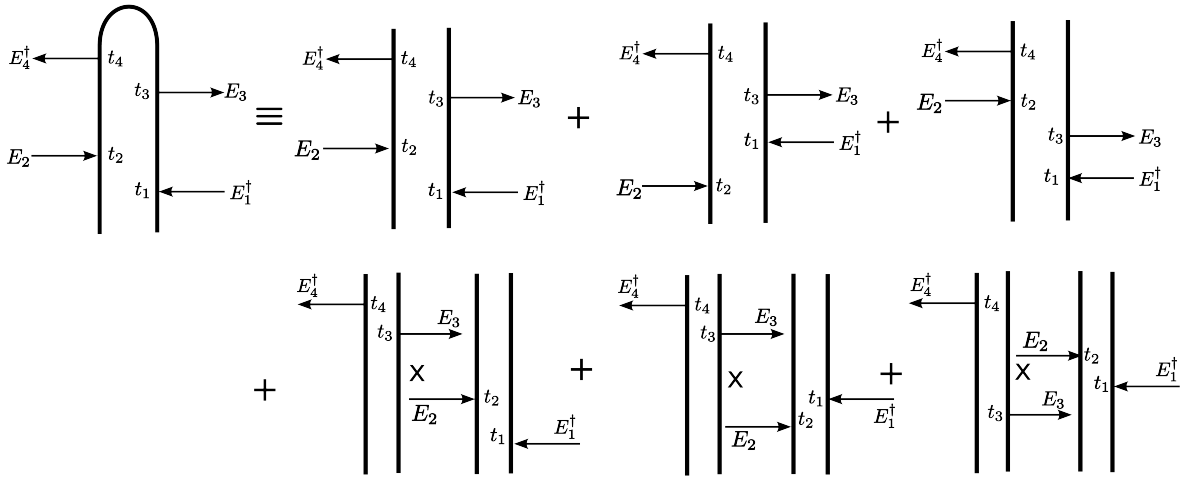

Figure S4: Ladder diagrams corresponding to a loop diagram for excited state emission (ESE). The top row shows complete diagrams, while the bottom row shows disconnected diagrams.

Excited state emission (ESE) contribution is probed by detecting two photons in D_i and zero photons in D_s, and the signal is defined as,

$$S_{ESE} = \frac{1}{2!}\left\langle \mathbf{T}\Omega_i^2 e^{-\Omega_i} \right\rangle \tag{S11}$$

The signal can be derived by following the steps in the GSB signal derivation, and the final

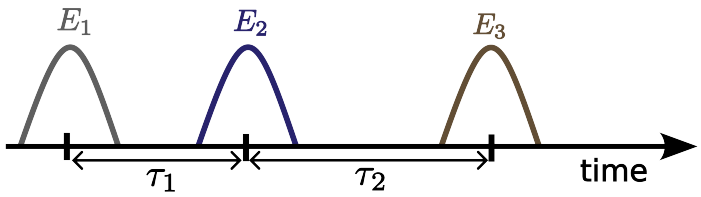

Figure S5: The pulse configuration for the 2DEVS technique. E_1 and E_2 are optical pulses that drive electronic transitions, and E_3 is an IR pulse that probes the non-linear response of the molecule. The optical and IR are considered to be temporally well-separated in our study.

expression reads,

$$\begin{aligned} S_{ESE} =& \frac{2}{\hbar^4}\Re\Bigg[\int_{-\infty}^{\infty}\mathrm{d}t_4\int_{-\infty}^{\infty}\mathrm{d}t_3\int_{-\infty}^{t_3}\mathrm{d}t_2\int_{-\infty}^{t_4}\mathrm{d}t_1\,\langle\psi_M|\,\hat{\mu}_2(t_2)\hat{\mu}_3^\dagger(t_3)\hat{\mu}_4(t_4)\hat{\mu}_1^\dagger(t_1)\,|\psi_M\rangle \\ &\times\langle\psi_F|\,\hat{E}_2^\dagger(t_2)\hat{E}_4^\dagger(t_4)\hat{E}_3(t_3)\hat{E}_1(t_1)\,|\psi_F\rangle \\ &+\int_{-\infty}^{\infty}\mathrm{d}t_4\int_{-\infty}^{\infty}\mathrm{d}t_3\int_{-\infty}^{t_4}\mathrm{d}t_2\int_{-\infty}^{t_3}\mathrm{d}t_1\,\langle\psi_M|\,\hat{\mu}_1(t_1)\hat{\mu}_3^\dagger(t_3)\hat{\mu}_4(t_4)\hat{\mu}_2^\dagger(t_2)\,|\psi_M\rangle \\ &\times\langle\psi_F|\,\hat{E}_1^\dagger(t_1)\hat{E}_4^\dagger(t_4)\hat{E}_3(t_3)\hat{E}_2(t_2)\,|\psi_F\rangle\Bigg] \end{aligned} \tag{S12}$$

Figure S4 shows a loop diagram for the ESE contribution along with corresponding ladder diagrams. The right-most diagram does not represent the actual ESE contribution and can be eliminated by introducing a delay between signal and idler photons that is much larger than the pulse width that creates entangled photons. The disconnected parts do not contribute to the ESEsignal since the contribution from $\hat{E}_3$ and $\hat{E}_4$ fields is vanishing in our system since it starts in the ground vibronic state.

The Classical 2DEVS Signal

2DEVS is a method based on the four-wave mixing technique, in which molecules interact with three pulses, which generates a non-linear response in the molecules, that results in the emission of a signal photon. The pulse configuration for the 2DEVS method is shown in Fig.

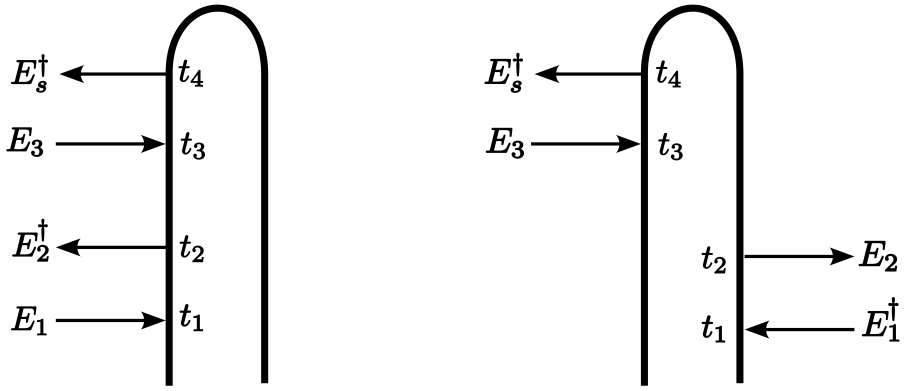

Figure S6: Loop diagrams corresponding to the GSB contribution to the 2DEVS signal. Each arrow indicates a light-matter interaction process.

S5. Two optical pulses are used to create electronic transitions in the molecules under study, while an IR pulse probes the response generated in the molecule. The signal photon can be seen as self-heterodyned with the third pulse, E_3.

The 2DEVS signal is defined as a change in the number of photons of the third light pulse,

$$S_{cl} = \int_{-\infty}^{\infty} \mathrm{d}t_4 \frac{\mathrm{d}}{\mathrm{d}t_4} \langle N_3(t_4) \rangle \tag{S13}$$

where $N_3{=}a_3^\dagger a_3$ represents the photon number operator for the third pulse, E_3, with a_3 ($a_3^\dagger$) being the corresponding annihilation (creation) operator. The above expression can be calculated using the time-dependent perturbation theory in the light-matter interactions. There are three contributions to the 2DEVS signal when the molecule is initially in a vibronic ground state ($|g,0\rangle$), namely, ground state bleach (GSB), excited state absorption (ESA), and stimulated emission (SE), and the total signal can be recast as,

$$S_{cl}(\tau_1,\tau_2) = S_{GSB}(\tau_1,\tau_2) + S_{ESA}(\tau_1,\tau_2) + S_{SE}(\tau_1,\tau_2) \tag{S14}$$

where τ_1 is the delay between E_1 and E_2, and τ_2 is the delay between E_2 and E_3. The GSB

contribution, S_{GSB}, is given by,

$$S_{GSB}(\tau_1,\tau_2) = 2\Re\int_{-\infty}^{\infty}\mathrm{d}t_4\int_{t_0}^{t_4}\mathrm{d}t_3\times$$
$$\left\{\int_{t_0}^{t_3}\mathrm{d}t_2\int_{t_0}^{t_2}\mathrm{d}t_1\,\langle\psi_T(t_0)|\,\mu_v(t_4)E_3^{\dagger}(t_4-\tau_2)\mu_v^{\dagger}(t_3)E_3(t_3-\tau_2)\mu_e(t_2)E_2^{\dagger}(t_2-\tau_1)\mu_e^{\dagger}(t_1)E_1(t_1)\,|\psi_T(t_0)\rangle + \right.$$
$$\left.\int_{t_0}^{t_4}\mathrm{d}t_2\int_{t_0}^{t_2}\mathrm{d}t_1\,\langle\psi_T(t_0)|\,\mu_e(t_1)E_1^{\dagger}(t_1)\mu_e^{\dagger}(t_2)E_2(t_2-\tau_1)\mu_v(t_4)E_3^{\dagger}(t_4-\tau_2)\mu_3^{\dagger}(t_3)E_3(t_3-\tau_2)\,|\psi_T(t_0)\rangle\right\} \tag{S15}$$

where $\psi_T(t_0)$ represents the total field + matter wave function at an initial time t_0, which will be set to $-\infty$ in our derivations later on. Note that we work in atomic units (i.e., $\hbar = e = m_e = 4\pi\epsilon_0 = 1$), unless stated otherwise. Figure S6 depicts the loop diagrams relevant to the GSB.

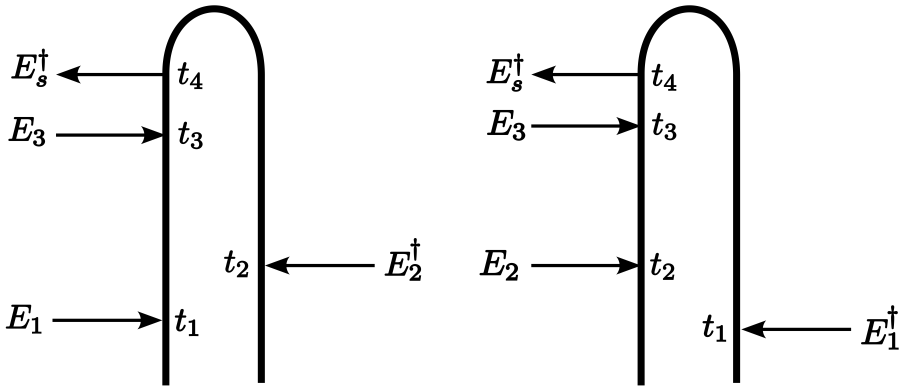

Figure S7: Loop diagrams corresponding to the ESA contribution to the 2DEVS signal. Each arrow indicates a light-matter interaction process.

Similarly, the ESA and SE contributions are given by,

$$S_{ESA}(\tau_1,\tau_2) = -2\Re\int_{t_0}^{\infty}\mathrm{d}t_4\int_{t_0}^{t_4}\mathrm{d}t_3\times$$
$$\left\{\int_{t_0}^{t_4}\mathrm{d}t_2\int_{t_0}^{t_3}\mathrm{d}t_1\,\langle\psi_T(t_0)|\,\mu_e(t_2)E_2^{\dagger}(t_2-\tau_1)\mu_v(t_4)E_3^{\dagger}(t_4-\tau_2)\mu_v^{\dagger}(t_3)E_3(t_3-\tau_2)\mu_e^{\dagger}(t_1)E_1(t_1)\,|\psi_T(t_0)\rangle + \right.$$
$$\left.\int_{t_0}^{t_4}\mathrm{d}t_1\int_{t_0}^{t_3}\mathrm{d}t_2\,\langle\psi_T(t_0)|\,\mu_e(t_1)E_1^{\dagger}(t_1)\mu_v(t_4)E_3^{\dagger}(t_4-\tau_2)\mu_v^{\dagger}(t_3)E_3(t_3-\tau_2)\mu_e^{\dagger}(t_2)E_2(t_2-\tau_2)\,|\psi_T(t_0)\rangle\right\} \tag{S16}$$

The loop diagrams corresponding to the ESA contribution to the 2DEVS signal are shown

in Fig. S7.

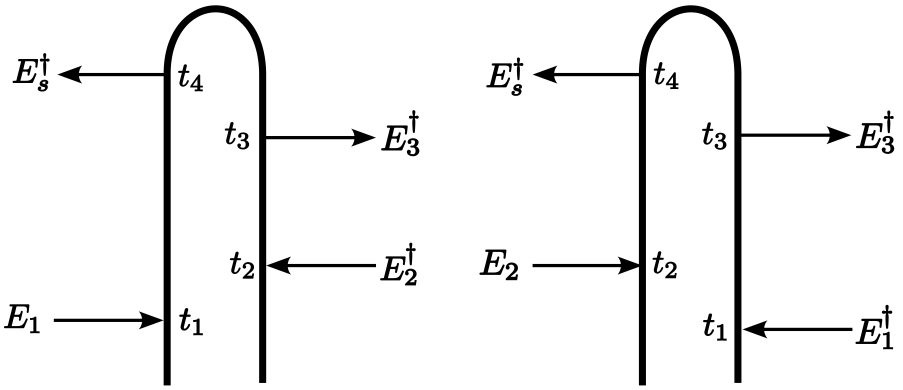

Figure S8: Loop diagrams corresponding to the SE contribution to the 2DEVS signal. Each arrow indicates a light-matter interaction process.

$$
\begin{aligned}
S_{ESE}(\tau_1,\tau_2) = 2\Re \int_{t_0}^{\infty} \mathrm{d}t_4 \int_{t_0}^{t_4} \mathrm{d}t_3 \times \\
\left\{ \int_{t_0}^{t_3} \mathrm{d}t_2 \int_{t_0}^{t} \mathrm{d}t_1 \, \langle \psi_T(t_0)| \, \mu_e(t_2) E_2^\dagger(t_2-\tau_1) \mu_v^\dagger(t_3) E_3(t_3-\tau_2) \mu_v(t_4) E_3^\dagger(t_4-\tau_2) \mu_e^\dagger(t_1) E_1(t_1) \, |\psi_T(t_0)\rangle + \right. \\
\left. \int_{t_0}^{t} \mathrm{d}t_2 \int_{t_0}^{t_3} \mathrm{d}t_1 \, \langle \psi_T(t_0)| \, \mu_e(t_1) E_1^\dagger(t_1) \mu_v^\dagger(t_3) E_3(t_3-\tau_2) \mu_v(t_4) E_3^\dagger(t_4-\tau_2) \mu_e^\dagger(t_2) E_2(t_2-\tau_1) \, |\psi_T(t_0)\rangle \right\}
\end{aligned}
\tag{S17}
$$

The loop diagrams corresponding to the ESE process in 2DEVS are shown in Fig. S8.

We construct frequency-dispersed signals by using the following frequency-domain expression for the signal field and omitting the integration over the frequency,

$$
E_3(t_4) = \int \mathrm{d}\omega_r E_3(\omega_r) e^{-i\omega_r t_4} \tag{S18}
$$

where $E_3(\omega_r)$ is the electric field in frequency-domain, and ω_r is the signal frequency. 2D frequency-dispersed spectra are constructed by Fourier transforming one of the time delays while using the other time delay as a parameter.